Effect of stacking fault energy on the thickness and density of annealing twins in recrystallized FCC medium and high-entropy alloys

Schneider, Mike; Couzinié, Jean Philippe; Shalabi, Amin; Ibrahimkhel, Farhad; Ferrari, Alberto; Körmann, Fritz; Laplanche, Guillaume

DOI
10.1016/j.scriptamat.2023.115844

Publication date
2024

Document Version
Final published version

Published in
Scripta Materialia

Scripta Materialia 240 (2024) 115844

Contents lists available at ScienceDirect

Scripta Materialia

journal homepage: www.journals.elsevier.com/scripta-materialia

Effect of stacking fault energy on the thickness and density of annealing twins in recrystallized FCC medium and high-entropy alloys

Mike Schneider [a,b,*], Jean-Philippe Couzinié [c], Amin Shalabi [b], Farhad Ibrahimkhel [b], Alberto Ferrari [d], Fritz Körmann [d,e,f], Guillaume Laplanche [b]

[a] PSL University, Chimie ParisTech, CNRS, Institut de Recherche de Chimie Paris, Paris 75005, France
[b] Institut für Werkstoffe, Ruhr-Universität Bochum, D-44801 Bochum, Germany
[c] Univ Paris Est Creteil, CNRS, ICMPE, UMR 7182, 2 rue Henri Dunant, Thiais 94320, France
[d] Materials Science and Engineering, Delft University of Technology, 2628CD Delft, the Netherlands
[e] Max-Planck-Institut für Eisenforschung GmbH, Max-Planck-Straße 1, D-40237 Düsseldorf, Germany
[f] Bundesanstalt für Materialforschung und -prüfung (BAM), Richard-Willstätter-Straße 11, D-12489 Berlin, Germany

ARTICLE INFO

Keywords:
CoCrFeMnNi HEAs and MEAs
Recrystallization
Transmission electron microscopy (TEM)
Electron backscatter diffraction
Grain boundary engineering

ABSTRACT

This work aims to predict the microstructure of recrystallized medium and high-entropy alloys (MEAs and HEAs) with a face-centered cubic structure, in particular the density of annealing twins and their thickness. Eight MEAs and five HEAs from the Cr-Mn-Fe-Co-Ni system are considered, which have been cast, homogenized, cold-worked and recrystallized to obtain different grain sizes. This work thus provides a database that could be used for data mining to take twin boundary engineering for alloy development to the next level. Since the stacking fault energy is known to strongly affect recrystallized microstructures, the latter was determined at 293 K using the weak beam dark-field technique and compared with ab initio simulations, which additionally allowed to calculate its temperature dependence. Finally, we show that all these data can be rationalized based on theories and empirical relationships that were proposed for pure metals and binary Cu-based alloys.

Annealing, growth and deformation twins are known to play an important role in the mechanical properties of face-centered cubic (FCC) metals and alloys. On the one hand, they can act as barriers against dislocation slip, e.g., nanotwinned Cu is ~10 times stronger than its coarse-grained counterpart while retaining a comparable electrical conductivity [1]. On the other hand, twins can act as sources of strain localization [2,3] and may serve as crack initiation sites during fatigue loading in austenitic stainless steels [4] and Ni-based superalloys [5]. From an engineering point of view, it is therefore important to control the microstructure of twinned materials and to identify the key parameters that allow this to be achieved.

In the case of recrystallized materials, various models have been proposed to rationalize the formation of annealing twins in FCC metals and alloys [6–12] and reviewed by Meyers and McCowan [13]. Since these models have only been applied to a limited number of pure metals and binary alloys so far, it is unclear, whether they can be used to predict the distribution and thickness of annealing twins in more complex solid solutions such as medium and high-entropy alloys (MEAs and HEAs). The present work therefore aims to fill this gap. In addition, the microstructural and physical parameters, as well as the methods used to obtain them, are not systematically reported in this field of research, which hinders the comparability of the data, and more importantly, prevents *data mining* to take *twin boundary engineering* in alloy development to the next level [14,15]. Therefore, the second objective of the present study is to provide a comprehensive database of annealing twin microstructures in single-phase FCC recrystallized MEAs and HEAs from the Cr-Mn-Fe-Co-Ni system.

Cylindrical 2.1 kg ingots of five equiatomic MEAs (CoNi, FeCoNi, MnCoNi, CrFeCoNi, and MnFeCoNi) were cast and homogenized between 1373 K and 1473 K for 48 h in evacuated quartz tubes as described in [16]. To verify the chemical homogeneity and purity of these alloys, EDX mappings were recorded in the as-cast and homogenized states, and compositions and impurity concentrations were measured at a commercial laboratory (Revierlabor Essen, Germany), see Figs. S1–S8 and Table S1 of the supplementary materials file. The alloys proved chemically homogeneous after annealing with relatively small impurity contents and compositions close to those desired (see Table S1). The homogenized ingots were then rotary swaged using the procedure

* Corresponding author at: Institut für Werkstoffe, Ruhr-Universität Bochum, D-44801 Bochum, Germany.
E-mail address: mike.schneider@rub.de (M. Schneider).

https://doi.org/10.1016/j.scriptamat.2023.115844
Received 12 August 2023; Received in revised form 6 October 2023; Accepted 23 October 2023
Available online 7 November 2023

reported in [17] and recrystallized between 773 K and 1573 K for 30 min to 120 min, yielding different grain sizes and distributions of annealing twins. In addition to the aforementioned alloys, MEAs and HEAs, which we had previously investigated using the same processing route and characterization methods, were considered here, i.e., MnFeNi [16,18], CrCoNi [19,20], CrFeNi [21,22], and five $Cr_xMn_{20}Fe_{20}Co_{20}Ni_{40-x}$ HEAs with $x = 14$, 18, 20, 22, and 26 at.% [23], which are labelled Cr_{14}, Cr_{18}, Cr_{20}, Cr_{22}, and Cr_{26}, respectively. As this database includes eight MEAs and five HEAs with a broad range of properties (shear modulus, SFE and lattice parameter), it may be used to determine how these affect the recrystallized microstructure of FCC materials.

After recrystallization, specimens were prepared for metallographic examinations following Ref. [19]. Texture analyses were performed along the longitudinal axis of the swaged rods using electron backscatter diffraction (EBSD) in a Quanta FEI 650 ESEM equipped with a Hikari XP camera (EDAX, AMETEK). These are presented as inverse pole figures (IPFs) averaged over ~300 grains, where the textures are expressed as multiples of random (see Figs. S9–S13). In most cases, these results revealed that the recrystallized materials do not exhibit a pronounced texture, see also [24].

From backscatter electron (BSE) and optical micrographs, the Heyn intercept method outlined in ASTM E-112 [25] was employed to determine the arithmetic mean grain size (d, excluding annealing twin boundaries) and crystallite size (c, taking into account both grain and annealing twin boundaries), which are defined as mean intercept distances[1] (no correction factor was involved). Detailed annealing conditions of the five alloys of the present study and resulting grain size distributions can be found in section D of supplementary materials (see Tables S2–S21, and Figs. S14 and S15) and in Refs. [18,20,22,23] for CrCoNi, CrFeNi, MnFeNi and the five HEAs, respectively. Using the values of d and c, the density of annealing twins n, defined as the number of annealing twin boundaries per grain, was calculated using:

$$n = \frac{d}{c} - 1 \tag{1}$$

The n-values directly obtained by EBSD and those calculated with Eq. (1) are compared in Fig. S16, which reveals a reasonable agreement between both methods. In the remainder of this article, we only consider the n-values obtained with the latter since it involved a greater number of analyzed grains.

The mean annealing twin thickness t was determined following the methodology outlined in Ref. [19]. Please note that this represents an average thickness projected on the sample surface, which is therefore larger than the real mean thickness of the twin lamellae. Finally, note that all microstructural values were obtained using the same procedures, thus allowing for a fair comparison.

The SFE determination of CrFeCoNi and MnFeCoNi ($d \approx 10$ μm) was performed from specimens (diameter: 4 mm, height: 8 mm) compressed at 293 K to 1–3 % plastic strain with a strain rate of 10^{-3} s^{-1}. Samples were then sliced at 45° from the loading axis, ground and electropolished to produce specimens for transmission electron microscopy (TEM). In a grain with a surface normal close to ⟨111⟩, apparent separation distances between Shockley partials were measured using the weak beam dark-field (WBDF) technique in a FEI Tecnai F20 Super-Twin instrument operated at 200 kV. From the observed distances, the actual separations were corrected using the procedure recommended by Cockayne [26,27]. For the CrFeCoNi MEA, Shockley partial separations were successfully analyzed using the $g(3g)$-diffraction condition. In contrast, as this distance was very small in MnFeCoNi, a $g(4g)$-diffraction condition was used to improve the sharpness of the dislocations in the WBDF micrographs.[2] Finally, assuming elastic isotropy, the SFEs were deduced from the Shockley partials separations using Eq. S1 [29].

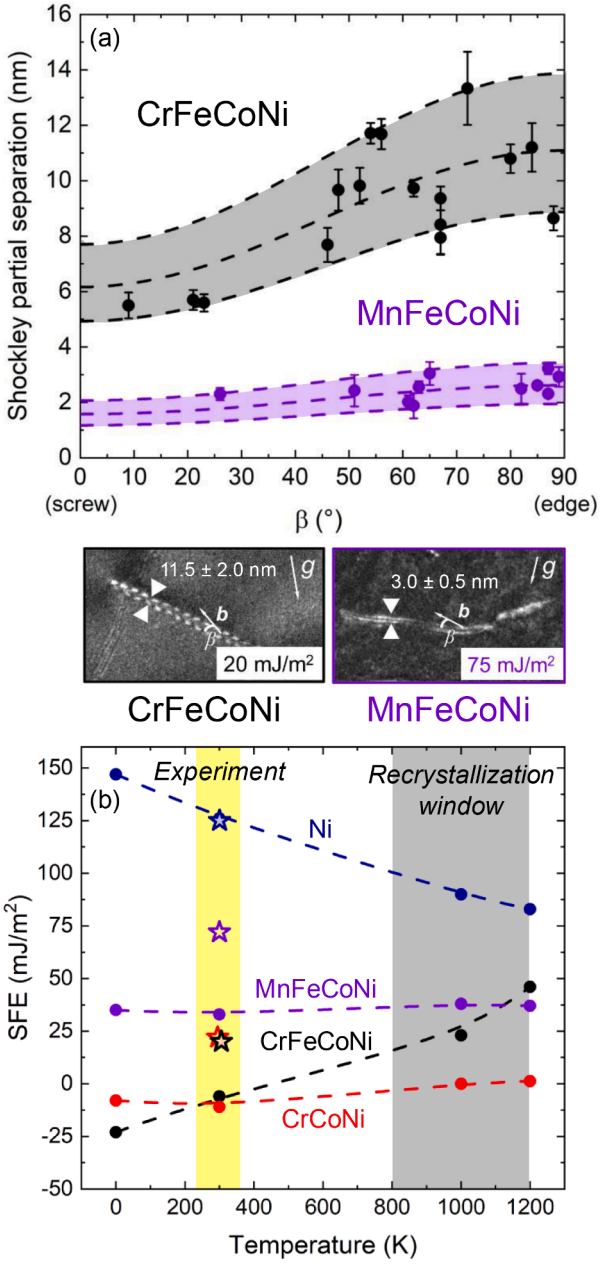

Fig. 1. Experimental SFE determined at 293 K and comparison with ab initio calculations between 0 and 1200 K. (a) Distance between Shockley partials versus screw/edge character β for CrFeCoNi and MnFeCoNi. Selected Shockley partial pairs for CrFeCoNi and MnFeCoNi are shown in the WBDF micrographs below (a). (b) SFE(T)-curves (dashed lines) of Ni and three MEAs calculated with the EMTO method in the ferromagnetic (Ni at 0 K and 293 K) and paramagnetic state otherwise. Experimental data at 293 K are represented by open stars (those for CrFeCoNi and CrCoNi were slightly shifted along the x-axis to avoid clutter). The yellow and grey backgrounds in (b) highlight the experimental data and the temperature range, in which recrystallization was conducted, respectively.

[1] EBSD was also used to determine the mean grain and crystallite sizes. The obtained values were in reasonable agreement with those obtained with the Heyn intercept method. Since more grains were evaluated with the latter approach, the values reported in the remainder of this article correspond to the Heyn intercept method.

[2] Since the effective extinction distance strongly decreases with increasing diffraction order, the analysis can only be performed in very thin parts of the TEM foil [28].

Table 1
Microstructural parameters S_{tvsd} and n, as well as *SFE* determined using the WBDF technique or computed with the EMTO method at different temperatures.

Temperature	S_{tvsd}	n	SFE_{TEM} (mJ/m^2) 293 K	*Ref. (SFE)*	SFE_{EMTO} (mJ/m^2) 0 K	293 K	[1000–1200] K
Ni	0.32 [11]	0.25 [12]	125 ± 30	[35]	147	126	87
CoNi	0.22 ± 0.02	1.17 ± 0.08	44	[36]	10	4	−9
			37	[37]			
			31	[38]			
CrFeNi	0.17 ± 0.01 [21]	0.90 ± 0.10	45 ± 7	[32]	−25	11	2
			37	[39]			
			52	[40]			
CrCoNi	0.13 ± 0.01 [19]	1.50 ± 0.12	22 ± 3	[31]	−8	−11	1
			18 ± 3	[33]			
FeCoNi	0.31 ± 0.01	1.03 ± 0.05	87*	–	53	54	56
MnFeNi	0.31 ± 0.01 [16]	0.49 ± 0.07	73*	–	45	40	43
MnCoNi	0.14 ± 0.03	0.86 ± 0.03	72*	–	52	39	36
CrFeCoNi	0.16 ± 0.02	1.20 ± 0.04	20 ± 4	present study	−23	−6	34
			27 ± 4	[33]			
MnFeCoNi	0.24 ± 0.01	0.66 ± 0.03	75 ± 17	present study	35	33	38
$Cr_{14}Mn_{20}Fe_{20}Co_{20}Ni_{26}$	0.20 [23]	0.37 ± 0.08	69 ± 13	[30]	−12	10	22
$Cr_{18}Mn_{20}Fe_{20}Co_{20}Ni_{22}$	0.18 [23]	0.44 ± 0.18	44 ± 8	[30]	−39	−2	12
$Cr_{20}Mn_{20}Fe_{20}Co_{20}Ni_{20}$	0.19 [23]	0.52 ± 0.08	35 ± 9	[30]	−55	−7	7
$Cr_{22}Mn_{20}Fe_{20}Co_{20}Ni_{18}$	0.19 [23]	0.51 ± 0.08	36 ± 10	[30]	−70	−11	5
$Cr_{26}Mn_{20}Fe_{20}Co_{20}Ni_{14}$	0.17 [23]	0.66 ± 0.11	21 ± 4	[30]	−95	−19	−2

* Values obtained by calculating the mean deviation between experimental and calculated results at 293 K of the MEAs and HEAs (~33 mJ/m^2, see Fig. S18) and adding this offset to the EMTO results.

While we had previously reported the SFEs of 4 HEAs [30] and 2 MEAs (CrCoNi [31] and CrFeNi [32]), those of CoNi and FeCoNi could not be measured due to the strong magnetism of these alloys, which rendered TEM investigations nearly impossible. Regarding MnFeNi and MnCoNi, attempts were made that were not successful so far.

From a fundamental viewpoint, the SFE that is relevant for the nucleation and growth of annealing twins during recrystallization should be determined at the temperature (T) at which twins grow. As it is experimentally very difficult to determine the Shockley partial separation in-situ, SFE(T)-curves were determined by ab initio simulations. The latter were performed to calculate the SFEs of all the previously mentioned materials (+Ni) at 0 K, 293 K, 1000 K and 1200 K. For this purpose, electronic structure calculations were performed within the density functional theory framework with the exact-muffin-tin-orbital (EMTO) method, following the procedure described in section E of supplementary materials.

The distance between Shockley partials determined from WBDF micrographs is shown in Fig. 1(a) as a function of β (angle between dislocation line and Burgers vector of the full dislocation) for MnFeCoNi and CrFeCoNi. Using a weighted least squares method, Eq. S1 was fitted to the two data sets and yielded SFEs of 75 ± 17 mJ/m^2 for MnFeCoNi and 20 ± 4 mJ/m^2 for CrFeCoNi. The latter value compares well with those reported in the literature (27 ± 4 mJ/m^2 [33] and 20 ± 4 mJ/m^2 [34]) using the same technique.

The SFE was calculated using the EMTO method between 0 K and 1200 K and representative examples (Ni, MnFeCoNi, CrFeCoNi, and CrCoNi) are compared to the experimental 293-K SFEs in Fig. 1(b). The full set of calculated SFE(T)-data are summarized in Table 1 and displayed in Fig. S17. Except for Ni, calculated SFEs systematically underestimate the experimental ones by ~33 mJ/m^2, see Fig. 1(b),

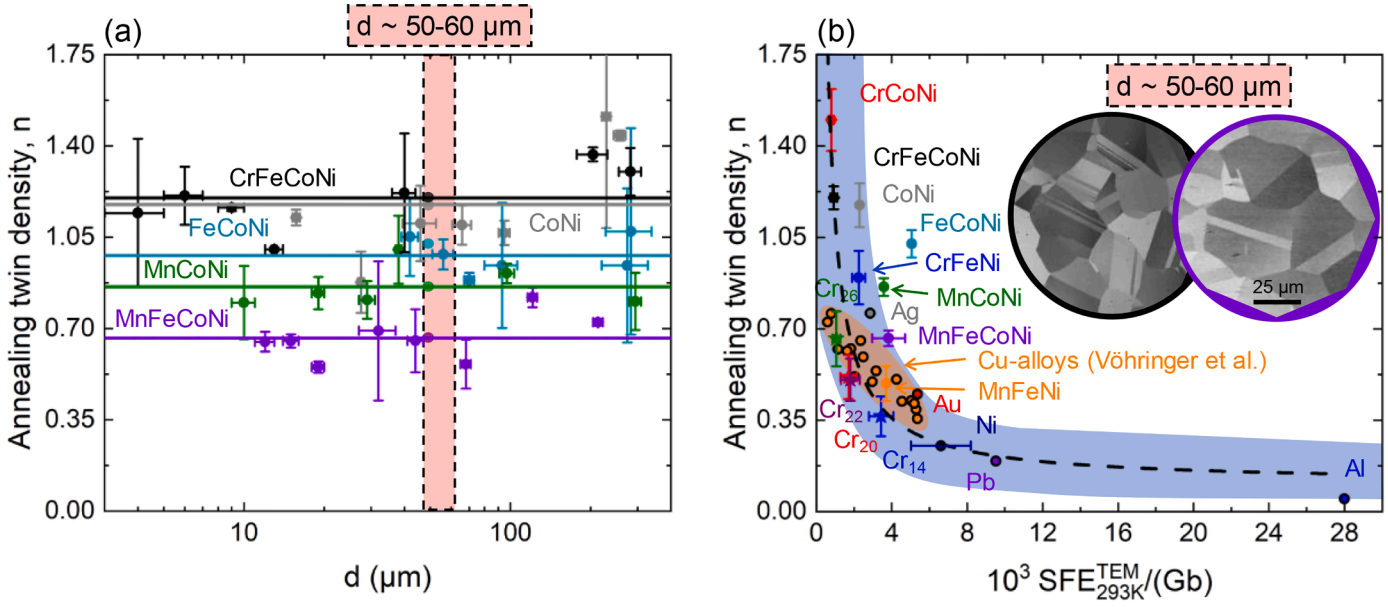

Fig. 2. (a) Annealing twin density n versus mean grain size d. The red region in (a) represents the grain size range: 50–60 µm. (b) Annealing twin density for 50 ≤ d ≤ 60 µm as a function of normalized experimental SFE for MEAs and HEAs (this work) as well as pure FCC metals [13] and binary Cu-alloys [12]. The black dashed line in (b) was fitted to the experimental data using the empirical relationship given in Eq. (2) and the blue area represents the scatter.

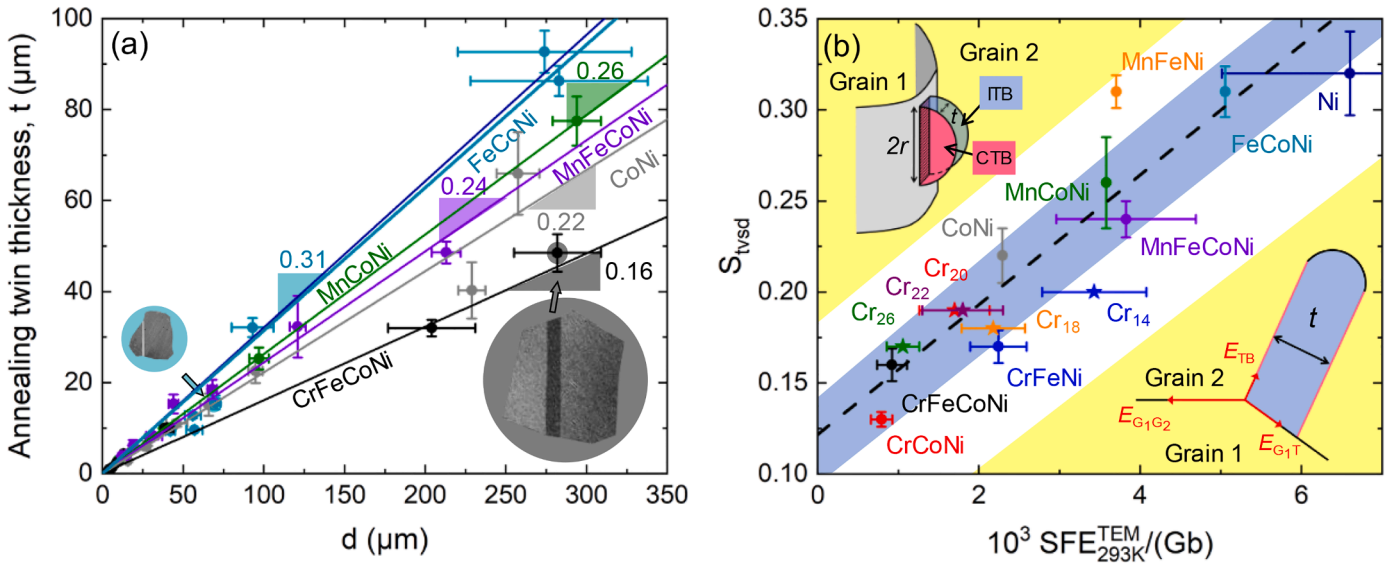

Fig. 3. (a) Annealing twin thickness t as a function of mean grain size d. Selected grains with thin and thick annealing twins are provided as insets in (a). Straight lines going through the origin were fitted to each data set in (a) and the corresponding slopes, S_{tvsd}, are displayed in (b) as a function of SFE/(Gb) (see also Table 1). The insets in (b) illustrate the Dash and Brown model for the growth of annealing twins at a migrating grain boundary [10], including coherent (CTB) and non-coherent twin interfaces (ITB). For more details see text.

Fig. S18, and Table 1. Possible rationales for this offset have been discussed in detail in [30]. The SFE(T)-curves in Fig. 1(b) are found to strongly depend on the material, e.g., the SFE of CrFeCoNi strongly increases with increasing T while those of MnFeCoNi and CrCoNi remain nearly constant and that of Ni strongly decreases. As a result, the difference between the SFEs is much lower at 1200 K than at 0 K.

Since, to our knowledge, no experimentally determined SFEs have been reported for FeCoNi, MnFeNi and MnCoNi to date, another approach was chosen to empirically correct the EMTO values obtained for these three alloys. As shown in Fig. S18, a systematic offset of ~33 mJ/m^2 was found at 293 K between experimentally determined and computed SFEs. Using this offset, estimates of experimental SFEs for FeCoNi, MnFeNi and MnCoNi were obtained by adding this offset to the EMTO results.

The number of annealing twin boundaries per grain n is shown in Fig. 2(a) as a function of d. Given experimental scatter, the n-value of each alloy can be considered as approximately independent of d when $d \leq 60$ μm. Interestingly, MnFeCoNi (SFE at 293 K: 75 mJ/m^2) and CrFeCoNi (SFE = 20 mJ/m^2) have high and low annealing twin densities, respectively, suggesting that n is related to the SFE, see Table 1.

In this context, the quantitative measurements, conducted by Vöhringer [12] in pure FCC metals and binary Cu-based alloys with $d \approx 50$ μm, are of considerable significance. To compare our data with those of Vöhringer, the conversion, described in section G of supplementary materials, was applied to account for the different relationships between c, d and n in Refs. [19] and [12]. In Fig. 2(b), n for $50 \leq d \leq 60$ μm is plotted as a function of the normalized SFE at 293 K (SFE/(Gb)), where G is the shear modulus and b the norm of the full Burgers vector. Given experimental scatters related to n and SFE values, it is surprising that the annealing twin boundary density of pure metals, binary alloys, MEAs and HEAs correlates well with the normalized SFE determined experimentally at 293 K using the following empirical relationship:

$$n = 0.108 + \left(\frac{Gb}{SFE}\right) \quad (2)$$

It is expected that this correlation should be better if one would consider the SFE at the recrystallization temperature (between 1000 K and 1200 K) instead of 293 K. To investigate this possibility, n is plotted as a function of SFE/(Gb) calculated at 0 K, 293 K, and 1000–1200 K in Figs. S19(a)–(c), respectively. The correlation between n and calculated SFEs in Fig. S19 is generally poorer than that obtained with the experimental ones determined at 293 K (Fig. 2(b)). This may be related to the difficulties and assumptions that are made to compute SFEs at finite temperatures. However, it is informative to see how the n-versus-SFE/(Gb)-curves evolve with increasing the temperature at which SFEs were computed. A comparison of Figs. S19(a), (b) and (c) reveals that, as expected, the scatter decreases with increasing temperature but this effect is mostly marked between 0 K and 293 K while the change between 293 K and 1200 K is relatively small. This may be one of the reasons for the surprisingly good correlation between the normalized SFE and n in Fig. 2(b). More importantly, the empirical relationship in Eq. (2) may be used to engineer the microstructure of recrystallized MEAs and HEAs.

The twin-thickness-versus-grain-size curves, $t(d)$, in Fig. 3(a) reveal that t is proportional to d. Straight lines were fitted to each data set to determine their slopes, S_{tvsd}. The proportionality between t and d in Fig. 3(a) is in excellent agreement with the annealing twin growth model proposed by Dash and Brown [10]. Even though this model was initially proposed for primary recrystallization (i.e., nucleation of dislocation-free grains that grow into a cold-worked matrix), Meyers and McCowan [13] suggested that this model could also be applied to secondary recrystallization (i.e., shrinkage of small grains to the benefit of large grains in a fully recrystallized microstructure). During secondary recrystallization, the migration of grain boundaries and triple points must be accommodated by deformation processes such as the nucleation and growth of annealing twins. The Dash and Brown model [10] considers a semi-circular annealing twin that has nucleated at a grain boundary and grows to decrease the overall interfacial energy of the system. The process is illustrated in the insets of Fig. 3(b) where side and top views are shown in the upper left and lower right corners, respectively. The radial growth of the annealing twin by dr induces a change in energy given by:

$$dE = [2\ t\ (E_{G_1T} - E_{G_1G_2}) + 2\ \pi\ r\ E_{CTB} + \pi\ t\ E_{ITB}]\ dr, \quad (3)$$

where E_{G_1T} and $E_{G_1G_2}$ are the interfacial energies between grain 1 and the annealing twin and grains 1 and 2, respectively. E_{ITB} and E_{CTB} are the surface energies of the incoherent and coherent twin boundaries, respectively. To minimize the overall interfacial energy (dE/dr) = 0, the equilibrium radius of the annealing twin is related to its thickness by:

$$r = -\frac{t}{2\,E_{\mathrm{CTB}}}\left[\frac{2}{\pi}\left(E_{\mathrm{G_1T}} - E_{\mathrm{G_1G_2}}\right) + E_{\mathrm{ITB}}\right]. \quad (4)$$

According to Eq. (4), spontaneous growth is only possible when $\frac{2}{\pi}(E_{\mathrm{G_1T}} - E_{\mathrm{G_1G_2}}) + E_{\mathrm{ITB}} < 0$. Assuming that SFE $\approx 2\,E_{\mathrm{CTB}}$ (in the absence of Suzuki effect [41]) and that the growth of an annealing twin ends when its radius becomes equal to the grain size d, Eq. (4) then implies that $t \propto d$, which is indeed what we observe in Fig. 3(a). According to the Dash and Brown model (Eq. (4)), the slopes S_{tvsd} of the lines shown in Fig. 3(a) should be proportional to $2\,E_{\mathrm{CTB}} \approx$ SFE. To investigate this possibility, Fig. 3(b) shows S_{tvsd} as a function of SFE/(Gb). Except for a small deviation for MnFeNi and some scatter, Fig. 3(b) shows that S_{tvsd} indeed increases linearly with increasing SFE ($S_{tvsd} = 0.122 + 0.036 \times$ SFE/(Gb)). The linear dependence shown in Fig. 3(b) has an ordinate intercept, unlike the Dash and Brown model [10]. However, it is worth recalling that the t-values in Fig. 3(a) are projected thicknesses of twin lamellae on the sample surface and are therefore larger than the real ones. Moreover, our mean grain sizes represent mean intercept lengths that are smaller than the corresponding average volumetric grain sizes, i.e., the latter is 1.571 times larger than the former [25]. We therefore argue that if these differences would be accounted for, the slopes of the t-versus-d plots in Fig. 3(a) would decrease by a constant ratio and the ordinate intercept of the fitted straight lines in Fig. 3(b) would be very close to zero, consistent with the model of Dash and Brown [10].

In Fig. S20, S_{tvsd} is shown as a function of the SFE, calculated within the EMTO framework at different temperatures. While using the SFEs calculated at 0 K (Fig. S20(a)) does not yield a good correlation, SFEs computed at RT (Fig. S20(b)) and at the recrystallization temperature (Fig. S20(c)) yield a better one, which is, given the uncertainties related to the simulations, in reasonable agreement with those obtained experimentally.

To summarize, the purpose of the present study was to investigate the effect of the SFE on the recrystallized microstructures of single-phase FCC MEAs and HEAs, focusing on the density and mean thickness of annealing twins. Interestingly, empirical relationships and theories that were proposed between the 60 s and 70 s for pure metals and binary Cu-based alloys also apply to MEAs and HEAs. These insights can thus be used to engineer the microstructure of recrystallized FCC materials regardless of their chemical complexity.

Declaration of Competing Interests

The authors declare that they have no known competing financial interests or personal relationships that could have appeared to influence the work reported in this paper.

Acknowledgments

M.S. acknowledges funding through a Feodor-Lynen Scholarship, granted by the Alexander von Humboldt foundation. G.L. acknowledges funding from the German Research Foundation (DFG) through project B8 of the SFB/TR 103. A.F. and F.K. acknowledge funding from the Nederlandse Organisatie voor Wetenschappelijk Onderzoek (NWO) [VIDI Grant No. 15707]. F.K. acknowledges the DFG via the Priority Program SPP 2006 “Compositionally Complex Alloys - High Entropy Alloys”. Part of the calculations were conducted on the Dutch national e-infrastructure with the support of SURF Cooperative.

Supplementary materials

Supplementary material associated with this article can be found, in the online version, at doi:10.1016/j.scriptamat.2023.115844.

References

[1] L. Lu, Y. Shen, X. Chen, L. Qian, K. Lu, Ultrahigh strength and high electrical conductivity in copper, Science 304 (5669) (2004) 422–426.
[2] J.C. Stinville, N. Vanderesse, F. Bridier, P. Bocher, T.M. Pollock, High resolution mapping of strain localization near twin boundaries in a nickel-based superalloy, Acta Mater. 98 (2015) 29–42.
[3] S. Pfeiffer, M.F. Wagner, Elastic deformation of twinned microstructures, Proc. Math. Phys. Eng. Sci. 473 (2017), 20170330.
[4] M.D. Roach, S.I. Wright, Investigations of twin boundary fatigue cracking in nickel and nitrogen-stabilized cold-worked austenitic stainless steels, Mater. Sci. Eng. A 607 (2014) 611–620.
[5] J.C. Stinville, W.C. Lenthe, J. Miao, T.M. Pollock, A combined grain scale elastic–plastic criterion for identification of fatigue crack initiation sites in a twin containing polycrystalline nickel-base superalloy, Acta Mater. 103 (2016) 461–473.
[6] R.L. Fullman, J.C. Fisher, Formation of annealing twins during grain growth, J. Appl. Phys. 22 (11) (1951) 1350–1355.
[7] H. Gleiter, The formation of annealing twins, Acta Metall. 17 (1969) 1421–1428.
[8] W.G. Burgers, `Stimulation crystals' and twin-formation in recrystallized aluminium, Nature 157 (1946) 76–77.
[9] M.A. Meyers, L.E. Murr, A model for the formation of annealing twins in F.C.C. metals and alloys, Acta Metall. 26 (1978) 951–962.
[10] S. Dash, N. Brown, An investigation of the origin and growth of annealing twins, Acta Mater. 11 (1963) 1067–1075.
[11] C.S. Pande, M.A. Imam, B.B. Rath, Study of annealing twins in FCC metals and alloys, Metall. Trans. A 21 (1990) 2891–2896.
[12] O. Vöhringer, Stapelfehlerenergie, Versetzungsdichte und -anordnung sowie Rekristallisations-Zwillingsdichte homogener Kupferlgierungen, Metall 26 (1972) 1119–1123.
[13] Meyers, M.A., McCowan, C. The Formation of Annealing Twins: Overview and New Thoughts, Interface Migration and Control of Microstructure, Detroit, American Society for Metals, USA (1984) 99–123.
[14] T.Z. Khan, T. Kirk, G. Vazquez, P. Singh, A.V. Smirnov, D.D. Johnson, K. Youssef, R. Arróyave, Towards stacking fault energy engineering in FCC high entropy alloys, Acta Mater. 224 (2022), 117472.
[15] G. Vazquez, P. Singh, D. Sauceda, R. Couperthwaite, N. Britt, K. Youssef, D. D. Johnson, R. Arróyave, Efficient machine-learning model for fast assessment of elastic properties of high-entropy alloys, Acta Mater. 232 (2022), 117924.
[16] M. Schneider, F. Werner, D. Langenkämper, C. Reinhart, G. Laplanche, Effect of temperature and texture on Hall–Petch strengthening by grain and annealing twin boundaries in the MnFeNi medium-entropy alloy, Metals 9 (2019) 84.
[17] G. Laplanche, O. Horst, F. Otto, G. Eggeler, E.P. George, Microstructural evolution of a CoCrFeMnNi high-entropy alloy after swaging and annealing, J. Alloys Compd. 647 (2015) 548–557.
[18] M. Schneider, F. Werner, D. Langenkämper, C. Reinhart, G. Laplanche, Data compilation on the effect of grain size, temperature, and texture on the strength of a single-phase FCC MnFeNi medium-entropy alloy, Data Brief 28 (2020), 104807.
[19] M. Schneider, E.P. George, T.J. Manescau, T. Záležák, J. Hunfeld, A. Dlouhý, G. Eggeler, G. Laplanche, Analysis of strengthening due to grain boundaries and annealing twin boundaries in the CrCoNi medium-entropy alloy, Int. J. Plast. 124 (2020) 155–169.
[20] M. Schneider, E.P. George, T.J. Manescau, T. Zalezak, J. Hunfeld, A. Dlouhy, G. Eggeler, G. Laplanche, Benchmark dataset of the effect of grain size on strength in the single-phase FCC CrCoNi medium entropy alloy, Data Brief 27 (2019), 104592.
[21] M. Schneider, G. Laplanche, Effects of temperature on mechanical properties and deformation mechanisms of the equiatomic CrFeNi medium-entropy alloy, Acta Mater. 204 (2021), 116470.
[22] M. Schneider, G. Laplanche, Data compilation regarding the effects of grain size, temperature, and texture on the strength of the single-phase FCC CrFeNi medium entropy alloy, Data Brief 34 (2020), 106712.
[23] C. Wagner, G. Laplanche, Effects of stacking fault energy and temperature on grain boundary strengthening, intrinsic lattice strength and deformation mechanisms in CrMnFeCoNi high-entropy alloys with different Cr/Ni ratios, Acta Mater. 244 (2023), 118541.
[24] G.Dan Sathiaraj, A. Pukenas, W. Skrotzki, Texture formation in face-centered cubic high-entropy alloys, J. Alloys Compd. 826 (2020), 154183.
[25] ASTM E112-10, Standard Test Methods for Determining Average Grain Size, ASTM International, West Conshohocken PA, USA, 2004.
[26] D.J.H. Cockayne, M.L. Jenkins, I.L.F. Ray, The measurement of stacking-fault energies of pure face-centred cubic metals, Philos. Mag. 24 (192) (1971) 1383–1392.
[27] D.J.H. Cockayne, A theorrtical analysis of the weak-beam method of electron microscopy, Z. Naturforsch. 27a (1972) 452–460.
[28] M.H. Loretto, R.E. Smallman, Defect Analysis in Electron Microscopy, Chapman and Hall, London, 1975.
[29] P.M. Anderson, J.P. Hirth, J. Lothe, Theory of Dislocations, third ed., Cambridge University Press, New York, USA, 2017.
[30] C. Wagner, A. Ferrari, J. Schreuer, J.-P. Couzinié, Y. Ikeda, F. Körmann, G. Eggeler, E.P. George, G. Laplanche, Effects of Cr/Ni ratio on physical properties of Cr-Mn-Fe-Co-Ni high-entropy alloys, Acta Mater. 227 (2022), 117693.
[31] G. Laplanche, A. Kostka, C. Reinhart, J. Hunfeld, G. Eggeler, E.P. George, Reasons for the superior mechanical properties of medium-entropy CrCoNi compared to high-entropy CrMnFeCoNi, Acta Mater. 128 (2017) 292–303.

[32] M. Rajkowski, M. Schneider, T. Gaag, N. Jöns, M. Münchhalfen, J. Schreuer, J.-P. Couzinié, G. Laplanche, Stacking fault energy, thermal expansion behavior and elastic stiffness coefficients of polycrystalline and single-crystalline CrFeNi medium-entropy alloys, in preparation.
[33] S.F. Liu, Y. Wu, H.T. Wang, J.Y. He, J.B. Liu, C.X. Chen, X.J. Liu, H. Wang, Z.P. Lu, Stacking fault energy of face-centered-cubic high entropy alloys, Intermetallics 93 (2018) 269–273.
[34] L. Li, Z. Chen, K. Yuge, K. Kishida, H. Inui, M. Heilmaier, E.P. George, Plastic deformation of single crystals of the equiatomic Cr-Fe-Co-Ni medium entropy alloy—A comparison with Cr-Mn-Fe-Co-Ni and Cr-Co-Ni alloys, Int. J. Plast. 169 (2023), 103732.
[35] C.B. Carter, S.M. Holmes, The stacking-fault energy of nickel, Philos. Mag. J. Theor. Exp. Appl. Phys. 35 (1977) 1161–1172.
[36] A.I. Salimon, A.M. Korsunsky, A.N. Ivanov, The character of dislocation structure evolution in nanocrystalline FCC Ni-Co alloys prepared by high-energy mechanical milling, Mater. Sci. Eng. A 271 (1999) 196–205.
[37] A. Howie, P.R. Swann, Direct measurements of stacking-fault energies from observations of dislocation nodes, Philos. Mag. 6 (1961) 1215–1226.
[38] M.H. Loretto, L.M. Clarebrough, R.L. Segall, Stacking-fault tetrahedra in deformed face-centred cubic metals, Philos. Mag. 11 (1965) 459–465.
[39] G. Bonny, D. Terentyev, R.C. Pasianot, S. Poncé, A. Bakaev, Interatomic potential to study plasticity in stainless steels: the FeNiCr model alloy, Model. Simul. Mater. Sci. Eng. 19 (2011), 085008.
[40] G. Bonny, N. Castin, D. Terentyev, Interatomic potential for studying ageing under irradiation in stainless steels: the FeNiCr model alloy, Model. Simul. Mater. Sci. Eng. 21 (2013), 085004.
[41] H. Suzuki, Segregation of solute atoms to stacking faults, J. Phys. Soc. Jpn. 17 (1962) 322–325.